Modeling of the burrowing mechanism by razor clam: role of penetration kinematics

Sichuan Huang¹ and Junliang Tao²

ABSTRACT

It has been reported that the Atlantic razor clam can burrow with an extremely high efficiency due to its well-evolved dynamic penetration kinematics. In general, the periodic penetration process is essentially an issue involving dynamic interaction between a shape-changing penetrator and the soil particles. In this paper, the three-dimensional Discrete Element Method (DEM) modeling method was used to preliminarily study the influence zone created by body expansion. The real penetrator was simplified as a two-body structure: a conical foot and a cylindrical body with a time-varying radius. To mathematically visualize the influence zone at different expansion conditions, distributions of average normal contact force and particle displacement across the sample are investigated. Results show that the expansion ratio and expanding rate have significant impact on the influence zone. Furthermore, a low lateral resisting force and large influence zone can be achieved by using a low expansion ratio and expansion coefficient.

Key word: burrowing, bio-inspired, shell expansion, penetration kinematics

INTRODUCTION

Many animals have evolved unique ways to locomote (e.g., swim, fly, run) in their habitat (water, air or ground) for survival. Most of the time, their locomotion strategies are efficient with low energy consumption. The Atlantic razor clams can efficiently penetrate into their substrate with a unique 'gait'. The penetration strategy of the razor clam has been literally described as a two-anchor system(Trueman 1967). As shown in Fig.1, the razor clam initialize the penetration with the expansion of its slender shell, compressing the surrounding soil to form a firm upper anchor; with the firm anchorage foot starts to probe downward until the maximum extension; contraction of the shells is then activated and the body liquid is pushed into the foot to form a bulbous terminal anchor; finally the shells are pulled downward with the terminal anchor; the razor clam returns to its initial state, preparing for the next penetration cycle. The muscle strength only allows the razor clam to drag its body downward with a tension force of 10N at most (Trueman 1967; Winter et al. 2012). Physically, such tension force can only enable the razor clam to submerge into the substrate for about 1~2 cm (Winter et al. 2012). However, the

¹Graduate Research Assistant, Department of Civil Engineering, University of Akron, OH 44325

²Assistant Professor, Department of Civil Engineering, University of Akron, OH 44325. Phone: (330)972-5932; Email: jtao2@uakron.edu

razor clam can dig up to 70 cm in reality (Holland and Dean 1977). In that case, the razor clam must manipulate the environment during penetration, which helps reduce the locomotion resistance and save energy. Penetration in soil is relevant to a great many geotechnical practices such as in-situ soil exploration, construction of tunnels, trenchless excavation, installation of piles and underground cables. It is envisioned that more sustainable and smart geotechnical solutions can be developed by learning from the penetration strategies adopted by burrowing animals. The first step is probably to understand the burrowing mechanisms from a soil mechanics point of view. Since a burrowing cycle by razor clams include multiple steps and complex interactions with the soil, it is necessary to first study the soil-clam interaction at each step.

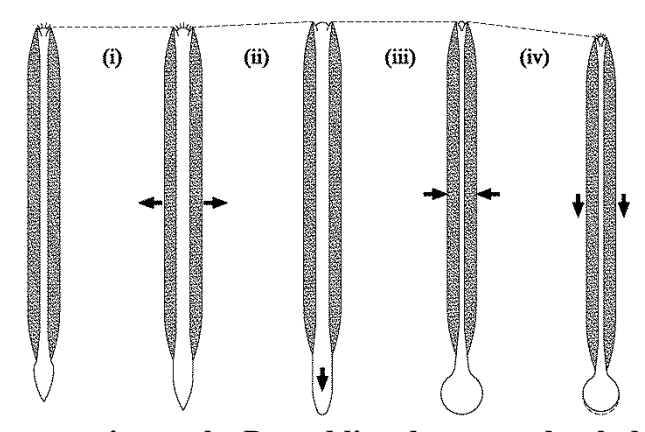


Figure 1. Razor clam penetration cycle. Dotted line denotes a depth datum. Arrow indicates the moving direction of foot and valves. (i) Expansion of valves. (ii) Foot probing downward. (iii) Valves adduction pushing water into foot to form a terminal anchor. (iv)Foot retraction, pulling downward valves and finally return to the initial stage, preparing for next cycle. (Trueman 1967)

The steps (iii) and (iv) in Fig. 1 have been studied previously. The clam shell contraction induced localized fluidization has been well accepted as the main source of locomotion resistance reduction and energy-saving. Trueman (1967) observed that water was ejected from the mantle cavity ventrally during shell contraction and induced the pressure rise around the clam. The ejected water was assumed to fluidize the substrate around the clam shell. Recently, the soil fluidization around the clam was successfully captured using high speed camera and Particle Image Velocimetry (PIV) technique (Winter et al. 2012). The pore pressure around the clam was asserted to drop at the shell contraction and cause the pore water inflow, which induced the following fluidization around the clam body. However, this conclusion was clearly refuted by the experiment data from Trueman (1967). A robotic clam-shape penetrator was also designed to capture the major locomotion kinematics (cyclic body expansion) during penetration, and results did demonstrated that the cyclic body expansion has positive reduction effect on the energy consumption upon locomotion (Winter et al. 2014). As an extension of the study, Isava and Winter have analytically demonstrated that the penetrator can move through the dry sand without lateral frictional resistance if the body can contract in 0.02s (Isava and Winter 2016).

Before shell contraction and retraction, shell expansion and foot expansion occur first. It is the penetration of the foot that dictates the net penetration. A clam cannot penetrate indefinitely into the ground and it is hypothesized that the penetration depth is primarily limited

by the capability of shell expansion and foot probing in soil. In order to achieve greater penetration depth, one hypothesis is that the expansion of the shell will cause stress relieve in the foot region so as to reduce the foot penetration resistance. Such a hypothesis is very similar to the crack propagation theory proposed in (Dorgan 2015), which discussed the mechanism of burrow extension in cohesive soil. But the role of expansion of shells on burrow extension in cohesion-less soil has not been elucidated and is the focus of this paper. In addition, the expanded shell serves as the anchor for the subsequent foot probing process. Therefore, the development of lateral force along the shell which dictates the anchoring force is also of interest in this study.

In this paper, the shell expansion process is simplified as a dynamic cylindrical cavity expansion issue. While analytical cavity expansion theory has been widely applied to study a various geotechnical processes, it can only provide approximate macroscale response. The discrete element method (DEM) has been demonstrated to be a useful alternative technique for the simulation of granular materials. With a basic constitutive law to express the interaction between two contacting phases, it can provide us a macroscopic/microscopic view of granules under dynamic perturbation (Cundall and Strack 1979). The DEM modeling approach has been successfully applied in the study of traditional cavity-expansion based penetration behaviors, such as cone penetration test (Butlanska et al. 2013; Falagush et al. 2015) and pressuremeter test (Geng et al. 2013) using commercial software, Particle Flow Code (PFC)(Itasca Consulting Group 2015); meanwhile, the DEM method was also successfully implemented for the simulation of the digging behavior within granular material in nature (Maladen et al. 2011). Their results all verified the feasibility of the application of the DEM method in capturing the soil-structure interaction patterns at multiple scales. Comparing to the traditional expansion theory, DEM is also more suitable for studies of dynamic soil-structure problems, like the burrowing process.

Only the influence of shell expansion characteristics upon the surrounding granular soil is studied in this paper. Other processes including the foot probing, shell contraction, foot anchorage are not considered but will be combined in the future work. Interested shell expansion characteristics include expansion ratio which represents how large the expansion amplitude is, as well as the expansion rate which represents how fast the expansion is. These characteristics will affect the surrounding soil in different ways, which will ultimately lead to different burrowing performances (i.e., anchoring efficiency, foot probing resistance, overall burrowing speed and efficiency). Therefore, it is critical to study the influence zone generated by the body expansion behavior so as to identify optimal expansion characteristics which maximize the burrowing performances.

METHODOLOGY

The commercial software, PFC 3D (version 5.00.22) was employed for the DEM simulation. The soil particles are modeled as spherical balls; the penetrator/cavity consists of rigid faceted walls, which are defined using a triangular mesh of facets. The Newton's law of motion is implemented to update the movement of the particles; the expansion of the faceted penetrator/cavity is realized by independently controlling the user-defined velocity of each vertex of the wall facets. The simple linear contact model is selected To model the particle-particle and particle-wall interactions (Itasca Consulting Group 2015). Since this study is not an attempt to model the penetration in a specific type of soil, idealized soil properties are used: the normal and tangential

stiffness of both particle and wall were set to be 5.0×10⁵ N/m; the frictional coefficient of particles was set as 0.7. A frictionless cylindrical chamber with an open top boundary was generated in a desired domain. The chamber diameter and height were both set to be 0.4 m, which were fixed during simulation. The granular sample with uniform particle size was generated with a target porosity of 0.40 using a radius expansion method, and was cycled to quasi-static state under the gravitational effect. The shape-changing penetrator was simplified as a two-body structure using faceted walls: a frictional conical wall with a fixed geometry and a frictional cylinder with a time-varying diameter. The cone tip had an apex angle of 60°. Both the cone and cylinder have an initial radius of 12 mm and a friction coefficient of 0.3. The penetrator was created at the center of the sample with a distance of 0.23 m from the chamber bottom to the cone tip. Particles within the generated faceted penetrator were then deleted. The final soil sample was obtained after a second round of cycling to quasi-static state.

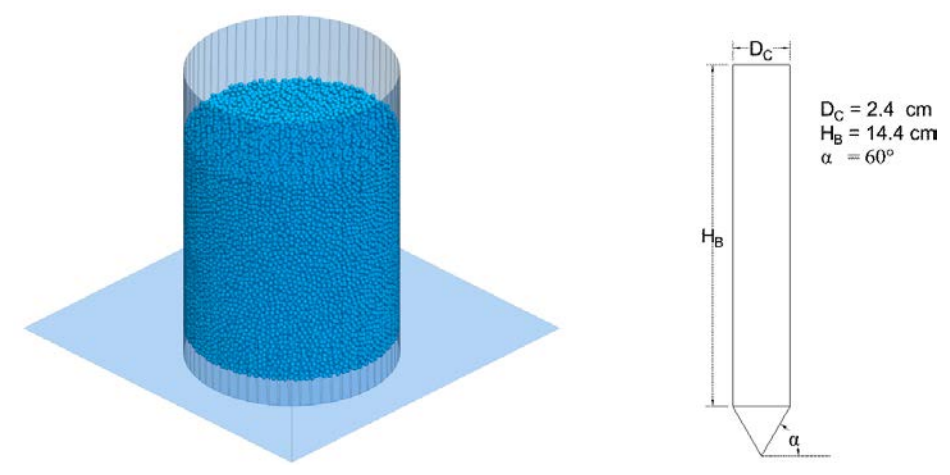


Figure 2. View of DEM model components (a) Soil sample (b) two-body penetrator

A built-in non-viscous damping scheme was employed to dissipate the additional kinetic energy of the particles and establish an equilibrium state during the soil sample preparation. The non-viscous local damping was removed when the sample was prepared. A contact-model-based damping strategy was then adopted to model the viscous behavior of the interactions among the particles and wall. Details of the input soil properties and contact parameters adopted in the simulation are summarized in Table 1.

Table 1. Input parameters for the numerical simulation				
Particle	unit			
Number	\	58439		
Diameter	m	1.0e-2		
Normal stiffness(<i>kn</i>)	N/m	5.0e5		
Tangential stiffness(ks)	N/m	5.0e5		
Friction coefficient	\	0.7		
Wall				
Normal stiffness(<i>kn</i>)	N/m	5.0e5		
Tangential stiffness(ks)	N/m	5.0e5		
Friction coefficient	\	0.3 for penetrator; 0.0 for external boundary		

Table 1. Input parameters for the numerical simulation

Two parameters were used to control the shell expansion dynamics: the body expanding rate described how fast the expansion is and is defined as the product of an expansion coefficient and the sample diameter; the expansion ratio describes how large the expansion amplitude is and is defined as the ratio of cylinder radius change over the initial cylinder radius. Different cylinder expansion ratios and expansion rates were considered, as listed in Table 2. In real case, the shell gape at the expansion is about 20°, which is equivalent to an approximate increment of 0.83 cm in thickness, or a expansion ratio of 0.2 for a clam with a shell length of 14.4 cm and a width of 2.4 cm (Trueman 1967). According to the time scale for each penetration stage recorded by (Trueman 1967), the equivalent expanding rate is about 0.0073 m/s or a corresponding expansion coefficient is about 0.0183. These numbers were used in Group #6 as a comparison basis.

Table 2. Simulation groups for the current study

	Expansion Ratio ^a	Expansion coefficient ^b (1/s)
Group #1	0.2	0.1
Group #2	0.3	0.1
Group #3	0.4	0.1
Group #4	0.2	0.2
Group #5	0.2	0.3
Group #6	0.2	0.0183
Group #7	0.2	0.0116

^aBody expanding rate = Expansion coefficient · Sample Diameter

RESULTS

Effects of expansion characteristics on lateral normal force on the shell

Lateral normal force is of interest in study of burrowing since animals spend energy when creating cavities and more importantly, through expanding the shell and the corresponding increase of the lateral normal force on it, the shell can serve as the anchor for the subsequent probing/penetrating events. Fig. 3 shows the lateral resisting force applied on the penetrator during body expansion for different expansion ratios and coefficients. In general, a relatively high lateral resisting force appears at the initiation of body expansion and progressively decreases until a transition point was achieved. The appearance of the initial high resisting force was expected due to the external force requirement for the sudden change of the surrounding particles from an initial quasi-static to a dynamic state. The resisting force then gradually increase till the end of expansion. At the same expansion rate, the development of the lateral contact force on the shell with a larger expansion ratio is just a continuation for that with a smaller expansion ratio. (Fig. 3a). With the same expansion ratio, different expansion coefficients result in different lateral resisting forces (Fig. 3b). A higher expanding rate means a more dramatic change and thus results in a higher initial resisting force. As shown in Fig. 3b, a low initial resisting force was recorded when a low expansion coefficient was implemented (Cases 6 and 7). On the other hand, a higher expansion coefficient also results in a more delayed appearance of the transition point. Fluctuations appear after transition point of lateral resisting force for each case, which was mainly due to the discrete nature of granular sample.

b*Expansion Ratio = (Final cylinder radius – initial cylinder radius) / initial cylinder radius

For live clams, the maximum haemocoele pressure recorded is about 10 kPa during locomotion. The increment of width after expansion is about 0.85 cm at the middle edge of shell for a razor clam with a shell of 14.4 cm in length and 2.4 cm in width. The maximum haemocoele pressure is equivalent to a lateral resisting force of approximate 76 N, which is comparable with that of numerical case (Group #6 and #7) in this study.

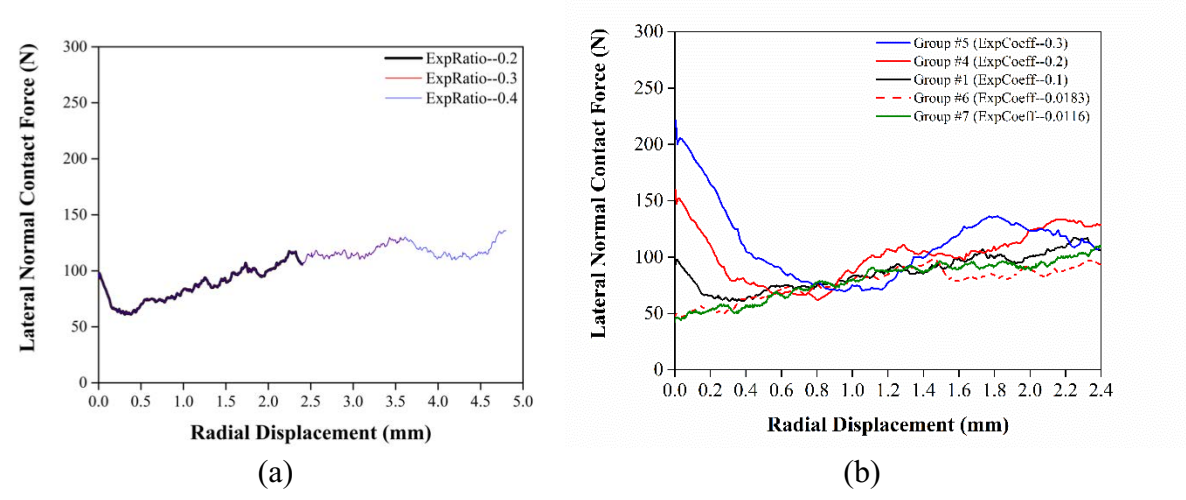


Figure 3. Lateral normal force applied on the body under different expansion rates (a) and coefficients (b)

Effects of expansion characteristics on disturbance of the soil states

The disturbance of the soil states due to shell expansion is also of interest since such changes will affect the subsequent burrowing steps. For a quantitative exploration of the influence zone generated by the body expansion, the particulate soil sample was divided into 15 stacks of cylindrical shell measurement regions in the radial direction and 35 stacks of cylindrical measurement regions in the vertical direction, as shown in Fig. 4. All the measurement regions are coaxial with the chamber and penetrator. Thickness of the measurement region was set to be the initial radius of the penetrator. The influence zone can then be quantitatively demonstrated through the distribution of the statistical average normal contact force and average particle displacement in the measurement regions.

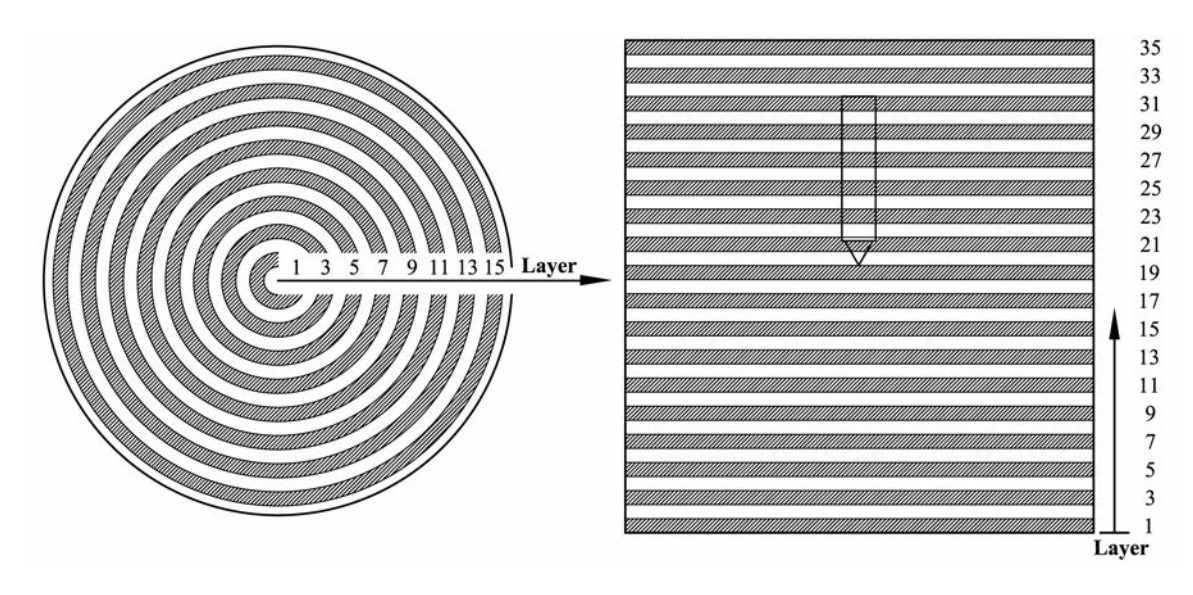


Figure 4. Measurement regions defined within the sample (a) cylindrical shell measurement regions defined in the radial/horizontal direction (b) cylindrical measurement regions defined in the vertical direction.

The average normal contact force was computed for each measurement region and each case. The normal force distribution of the initial state was also included for comparison. Fig. 5 presents data from cases with different expansion ratios. The normal force distribution of the initial state is relatively uniform in the horizontal direction, and linearly increases with increasing depth due to the increasing earth pressure. The body expansion compacted the surround soil and clearly caused an increase of average normal contact force across the sample in the horizontal direction (Fig. 5a). A local maximum normal force was detected within 2 body initial diameter from the sample center in the horizontal direction, and generally attenuated towards the sample external boundary. However, difference in average normal force for each measurement region between different cases is small in the horizontal distribution, which is due to the inclusion of particle gravitational effect.

In Fig. 5b, a local strong force concentration can be detected around the penetrator in the vertical direction. Such strong force concentration was progressively attenuated toward the top and bottom of the sample. Several interesting features can also be identified in the figure: (1) the vertical distribution of strong force network in areas around the penetrator is quite small; (2) difference among different distribution curves is distinguishable in area beneath the cone; with a higher expansion ratio, the average contact force for each measurement region becomes lower, and closer to the initial state; and (3) no clear difference among the distribution curves appears in area above the penetrator.

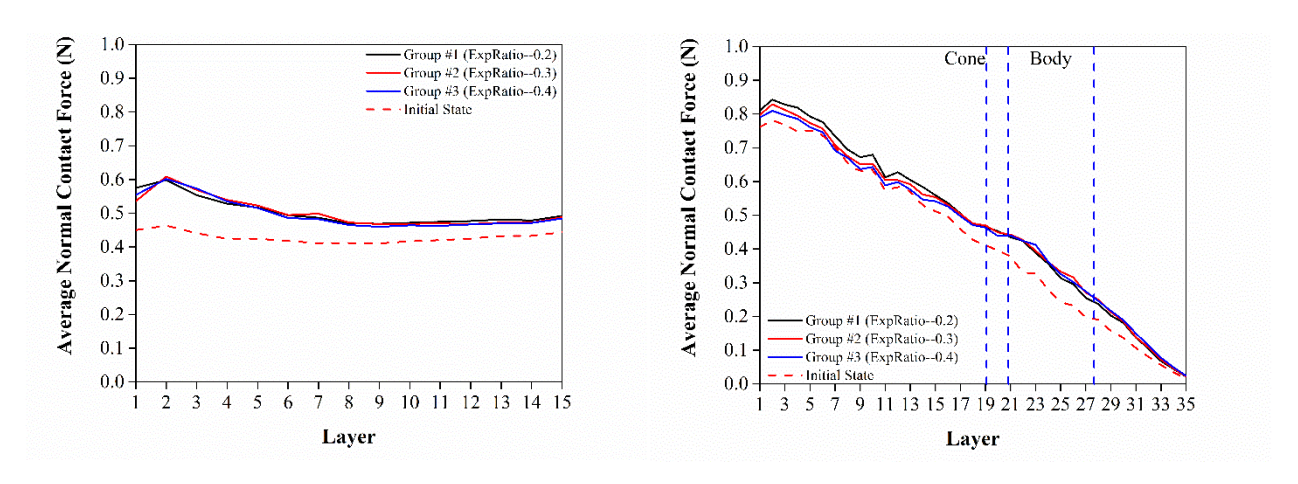


Figure 5. Normal contact force distribution for different expansion ratio (a) horizontal distribution (b) vertical distribution

The normal force distribution for different expansion coefficients is interesting (Fig.6). One significant common feature with Fig.5a is that a local strong force concentration was detected within two initial body diameters from sample center and progressively attenuated laterally (See Fig. 6a). On the other hand, the distribution curve with lower expansion coefficient becomes closer to the initial state at expansion coefficient lower than 0.2. For instance, a small strong force concentration appears when body expands with a coefficient of 0.083/s or 0.0116/s, which was soon attenuated towards the external boundary. For the force distribution for different expansion coefficient in vertical direction (Fig.6b), several interesting features are discernable. For all simulations, the depth dependency is similar, with a marked peak around the penetrator. However, their magnitudes differ with expansion coefficient. In general, with the smallest coefficient, the distribution curve of Group #7 is closest to the initial state. The distribution curves with a coefficient higher than 0.1/s all display a large difference with the initial state. Such difference was conveyed to the bottom of sample without significant attenuation. The distribution curve of Group #4 is the one that displays the largest difference with the initial state.

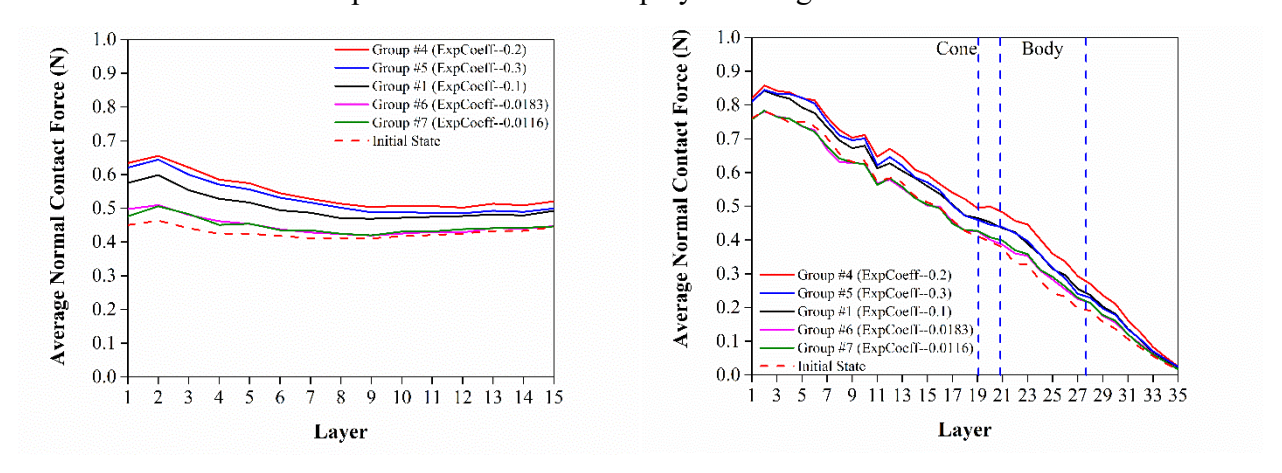


Figure 6. Normal contact force distribution for different expansion coefficient (a) horizontal distribution (b) vertical distribution

To further visualize the influence zone created by the body expansion, the average particle displacement for each measurement region is also recorded for each case, as shown in Fig.7 and Fig.8. Obviously, in all cases the largest displacement appears to occur close to the penetrator body. The smallest displacement occurs close to the external boundary wall. This phenomenon is consistent with the normal contact force distribution, whether in horizontal or vertical direction. For the distribution data with different expansion ratios (See Fig.7), a much more significant influence can be created by using a higher expansion ratio, and the disturbance around the penetrator is more marked than area around the external boundary.

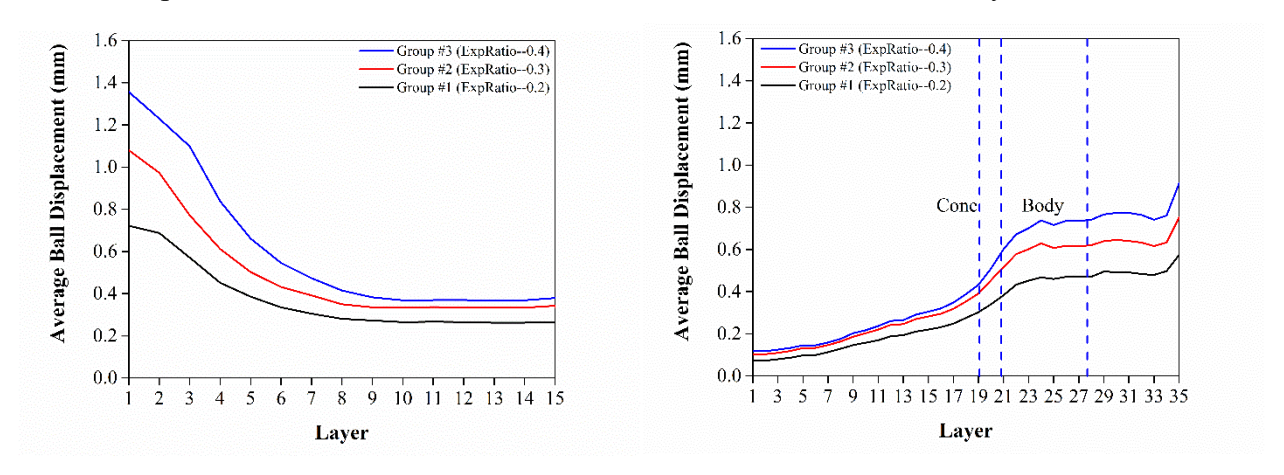


Figure 7. Particle displacement distribution under different expansion ratio (a) horizontal distribution (b) vertical distribution

Fig.8 provides a clear trend about the extent of influence corresponding to various expansion coefficient. Similar with Fig.7, a local significant influence area was detected around the penetrator. It is noteworthy that the higher the expansion coefficient is, the smaller average particle displacement achieved in each measurement region. In other word, body expansion induced disturbance upon the surrounding particle can be transferred further for a certain expansion ratio when a smaller expansion coefficient is implemented.

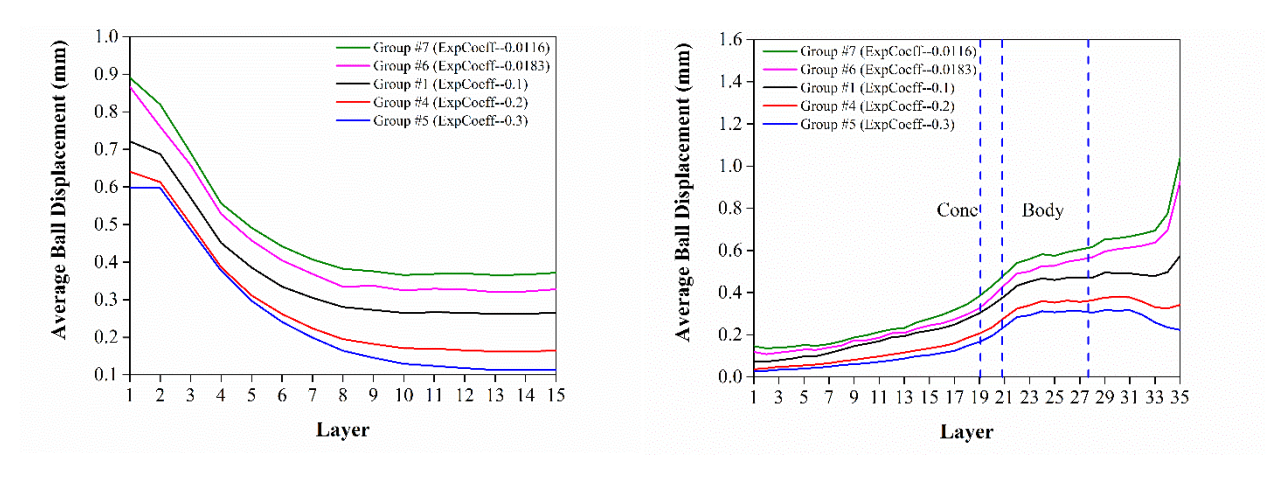


Figure 8. Particle displacement distribution under different expansion coefficient (a) horizontal distribution (b) vertical distribution

CONCLUSIONS

This paper adopted the numerical modelling approach to preliminarily study the influence zone created by expanding a cavity in granular soil. Different expanding expansion ratios and expansion rates were considered to explore the general evolution of influence zone and lateral resisting force under various loading conditions. Results demonstrated that the body expansion indeed affected the particulate environment around the penetrator. Furthermore, the expansion ratio and expanding rate were found to have significant impact on the influence zone and soil fabric. Results showed that a low lateral resisting force and larger influence zone can be achieved by a lower expansion ratio and expansion coefficient. In such a case, the expansion work can be minimized. But since burrowing efficiency (power) also depends on how fast the work is done, a minimized expansion energy doesn't warrant the maximized burrowing efficiency. In addition, the burrowing process is a complex soil-structure interaction problem involving multiple interdepended burrowing steps. The trends of soil disturbance observed in this study provide a basis for future studies on the interdependency of different burrowing steps.

REFERENCE

- Butlanska, J., Arroyo, M., Gens, A., and O'Sullivan, C. (2013). "Multi-scale analysis of cone penetration test (CPT) in a virtual calibration chamber." *Canadian Geotechnical Journal*, 51(1), 51-66.
- Cundall, P. A., and Strack, O. D. (1979). "A discrete numerical model for granular assemblies." *Geotechnique*, 29(1), 47-65.
- Dorgan, K. M. (2015). "The biomechanics of burrowing and boring." *J Exp Biol*, 218(Pt 2), 176-183. Falagush, O., McDowell, G. R., Yu, H. S., and de Bono, J. P. (2015). "Discrete element modelling and
- cavity expansion analysis of cone penetration testing." *Granular Matter*, 17(4), 483-495.
- Geng, Y., Yu, H., and McDowell, G. (2013). "Discrete element modelling of cavity expansion and pressuremeter test." *Geomechanics and Geoengineering*, 8(3), 179-190.
- Holland, A., and Dean, J. (1977). "The biology of the stout razor clamTagelus plebeius: I. Animal-sediment relationships, feeding mechanism, and community biology." *Chesapeake Science*, 18(1), 58-66.
- Isava, M., and Winter, A. G. (2016). "Razor clam-inspired burrowing in dry soil." *International Journal of Non-Linear Mechanics*, 81, 30-39.
- Itasca Consulting Group, I. (2015). "Guide book: theory and background PFC3D."
- Maladen, R. D., Ding, Y., Umbanhowar, P. B., and Goldman, D. I. (2011). "Undulatory swimming in sand: experimental and simulation studies of a robotic sandfish." *The International Journal of Robotics Research*, 30(7), 793-805.
- Richards Jr, R., Elms, D., and Budhu, M. (1990). "Dynamic fluidization of soils." *journal of Geotechnical Engineering*, 116(5), 740-759.
- Trueman, E. (1967). "The dynamics of burrowing in Ensis (Bivalvia)." *Proceedings of the Royal Society of London B: Biological Sciences*, 166(1005), 459-476.
- Winter, A. G., Deits, R. L. H., Dorsch, D. S., Slocum, A. H., and Hosoi, A. E. (2014). "Razor clam to RoboClam: burrowing drag reduction mechanisms and their robotic adaptation." *Bioinspiration & Biomimetics*, 9(3), 036009.
- Winter, A. G., Deits, R. L. H., and Hosoi, A. E. (2012). "Localized fluidization burrowing mechanics of Ensis directus." *Journal of Experimental Biology*, 215(12), 2072-2080.